Coherent Intrachain Energy Migration in a Conjugated Polymer at Room Temperature

Elisabetta Collini, *et al.*
Science **323**, 369 (2009);
DOI: 10.1126/science.1164016

ing the optical. By merging the nascent technique of transformation optics with traditional gradient-index optics, we have shown that more functional hybrid structures can be developed that enable us to access previously unseen electromagnetic behavior while mitigating some of the inherent limitations. Though transformation optical designs are highly complex, metamaterial implementations can be rapidly and efficiently achieved using the algorithms and approach described in this report.

References and Notes

1. J. B. Pendry, D. Schurig, D. R. Smith, *Science* **312**, 1780 (2006); published online 24 May 2006 (10.1126/science.1125907).
2. U. Leonhardt, *Science* **312**, 1777 (2006), published online 24 May 2006; 10.1126/science.1126493.
3. M. Rahm, S. A. Cummer, D. Schurig, J. B. Pendry, D. R. Smith, *Phys. Rev. Lett.* **100**, 063903 (2008).
4. M. Rahm *et al.*, *Opt. Express* **16**, 11555 (2008).
5. A. V. Kildishev, V. M. Shalaev, *Opt. Lett.* **33**, 43 (2008).
6. M. Rahm *et al.*, *Phot. Nano. Fund. Appl.* **6**, 87 (2008).
7. W. X. Jiang *et al.*, *Appl. Phys. Lett.* **92**, 264101 (2008).
8. Z. Ruan, M. Yan, C. W. Neff, M. Qiu, *Phys. Rev. Lett.* **99**, 113903 (2007).
9. A. Hendi, J. Henn, U. Leonhardt, *Phys. Rev. Lett.* **97**, 073902 (2006).
10. D. Schurig *et al.*, *Science* **314**, 977 (2006); published online 18 October 2006 (10.1126/science.1133628).
11. W. Cai, U. K. Chettiar, A. V. Kildishev, V. M. Shalaev, *Nat. Photon.* **1**, 224 (2007).
12. H. Chen, B. I. Wu, B. Zhang, J. A. Kong, *Phys. Rev. Lett.* **99**, 063903 (2007).
13. A. Alu, N. Engheta, *Phys. Rev. Lett.* **100**, 113901 (2008).
14. W. X. Jiang *et al.*, *Phys. Rev. E Stat. Nonlin. Soft Matter Phys.* **77**, 066607 (2008).
15. See the supporting material on *Science* Online.
16. J. Li, J. B. Pendry, *Phys. Rev. Lett.* **101**, 203901 (2008).
17. J. F. Thompson, B. K. Soni, N. P. Weatherill, *Handbook of Grid Generation* (CRC Press, Boca Raton, FL, 1999).
18. P. Knupp, S. Steinberg, *Fundamentals of Grid Generation* (CRC Press, Boca Raton, FL, 1994).
19. D. R. Smith, D. C. Vier, Th. Koschny, C. M. Soukoulis, *Phys. Rev. E Stat. Nonlin. Soft Matter Phys.* **71**, 036617 (2005).
20. R. Liu, T. J. Cui, D. Huang, B. Zhao, D. R. Smith, *Phys. Rev. E Stat. Nonlin. Soft Matter Phys.* **76**, 026606 (2007).
21. B. J. Justice *et al.*, *Opt. Express* **14**, 8694 (2006).
22. This work was supported by a gift from Raytheon Missile Systems (Tucson), and the rapid design approach was supported by a Multiple University Research Initiative supported by the Air Force Office of Scientific Research, contract no. FA9550-06-1-0279. T.J.C. acknowledges the support from InnovateHan Technology, National Science Foundation of China (60871016 and 60671015), National Basic Research Program (973) of China (2004CB719802), Natural Science Foundation of Jiangsu Province (BK2008031), and the 111 Project (111-2-05). We thank C. Harrison, N. Kundtz, and J. Allen for assistance for the experimental apparatus; A. Degiron for careful reading of the manuscript; Q. Cheng for the nonresonant element metamaterials technique development; and H. Schmitt, D. Barker (Raytheon Missile Systems), and M. West for helpful discussions.

Coherent Intrachain Energy Migration in a Conjugated Polymer at Room Temperature

Elisabetta Collini and Gregory D. Scholes*

The intermediate coupling regime for electronic energy transfer is of particular interest because excitation moves in space, as in a classical hopping mechanism, but quantum phase information is conserved. We conducted an ultrafast polarization experiment specifically designed to observe quantum coherent dynamics in this regime. Conjugated polymer samples with different chain conformations were examined as model multichromophoric systems. The data, recorded at room temperature, reveal coherent intrachain (but not interchain) electronic energy transfer. Our results suggest that quantum transport effects occur at room temperature when chemical donor-acceptor bonds help to correlate dephasing perturbations.

Numerous systems, such as natural photosynthetic proteins and artificial polymers, organize light-absorbing molecules (chromophores) to channel photon energy to create electronic or chemical gradients. The excitation energy from the absorbed light is either transferred through space or shared quantum mechanically among several chromophores (*1*). The interplay among these classical and quantum limits of electronic energy transfer (EET) dynamics is dictated by the way the chromophores communicate with each other via long-range Coulombic interactions, as well as by the strength of perturbations from the bath of fluctuating nuclear motions in the molecular architecture and surrounding external medium (*2–6*).

An elusive intermediate EET regime is of particular interest because the excitation moves in space—which is a deterministic, classical attribute—

Department of Chemistry, Institute for Optical Sciences, and Center for Quantum Information and Quantum Control, University of Toronto, Toronto, Ontario M5S 3H6, Canada.

*To whom correspondence should be addressed. E-mail: gscholes@chem.utoronto.ca

yet a preferred path can be adopted through wave function delocalization and associated interference effects, which introduce quantum characteristics to the dynamics (*7*). Together these attributes may in principle allow phase information to be transferred through space, with the electronic Hamiltonian of the entire system thereby steering EET. By learning how to observe the intermediate coupling case and thereafter to understand its properties, we could learn how to control excitation waves in a complex, multichromophoric system. Here, we present the results of an ultrafast spectroscopy experiment specifically designed to probe quantum coherent EET in the intermediate coupling case.

Rapid decoherence—the loss of memory of the initial electronic transition frequency distribution in an ensemble, caused by random fluctuations due to interaction of the system with its surroundings—is the primary reason for the scarcity of reports of coherent EET in complex condensed-phase systems. In the following, $|0\rangle$ designates the ground state, $|d\rangle$ is the donor, and $|a\rangle$ is the acceptor. According to theory, the evolution of

the acceptor probability density in EET can be written as a product of forward ($|d\rangle$ to $|a\rangle$) and reverse propagations of the system [e.g., (*2*)], which allows us to describe how the competition between electronic interaction and decoherence determines the EET dynamics. In the strong coupling case, the electronic coupling period dominates over decoherence; therefore, forward and reverse donor-acceptor paths tend to be almost identical. Phase is preserved over each path, and a kind of standing wave connects the two states so that their evolution is intimately entangled in a quantum state. In the weak coupling case, the fluctuations of the electronic transition frequency of a chromophore occur faster than the characteristic time of the donor-acceptor coupling. Owing to the tremendous number of different possible trajectories of transition energy fluctuations that can occur, the forward and reverse donor-acceptor propagations differ, so that decoherence dominates and the excitation is localized on the donor or acceptor at any one time—but not on both simultaneously—and the EET dynamics follow classical rate laws.

The rate of EET is often measured by transient absorption spectroscopy, where an ultrafast laser pulse photoexcites the donor chromophores and a probe pulse monitors the probability that the excitation has been transferred to an acceptor as a function of pump-probe delay time *T*. When the donor and acceptor chromophores have similar excitation energies, they cannot be spectrally distinguished, so we instead record anisotropy as a function of *T*. This technique has been extensively exploited to study EET in various kinds of multichromophoric systems (*8–10*). The anisotropy decay is caused by any process that changes the orientation of the chromophores probed relative to those initially photoexcited. For instance, electronic excitation could pass between two segments that are oriented at an angle in space. Alternatively, an excited chromophore could physically

rotate in the laboratory frame. In the experiments reported here, this latter rotational reorientation of the chromophores, which typically occurs on time scales of tens of picoseconds or longer, is far too slow to contribute to the first few hundred femtoseconds of the anisotropy decay.

The intermediate coupling case can be distinguished by determining whether phase information is retained in the $|d\rangle$ to $|a\rangle$ propagation when excitation is transferred. An experiment sensitive only to probability density, like the pump-probe methods mentioned above, cannot elucidate this question directly because that phase information is lost when populations are formed. Instead, we measure dynamics during a coherence time period τ when the system is in a superposition of ground and excited states, and we use anisotropy to signal quantitatively that excitation coherence has been transferred. The two-time anisotropy decay (TTAD) experiment measures coherent EET directly and thereby probes the memory, or degree of coherence, characteristic of the $|d\rangle$ to $|a\rangle$ forward propagation. Whether or not this process occurs is important to establish because it is often neglected in theory (the secular approximation).

More specifically, the TTAD is recorded as a function of two different time delays (τ and T) in a three-pulse heterodyne-detected transient grating experiment. The delay T is the population time, during which excited-state dynamics such as EET occur, whereas the phase-stable delay τ, introduced between the first two pulses, scans a time period when the system is in a coherence $|0\rangle\langle d|$ between the ground and excited electronic states (11). During the τ delay, the system undergoes dephasing (free induction decay) or coherent EET from $|0\rangle\langle d|$ to $|0\rangle\langle a|$. In TTAD, coherent EET is completely discriminated from the free induction decay by monitoring anisotropy. This τ regime is the time delay scanned in photon echo experiments, which we use to investigate whether coherent EET also occurs during the population time period.

We applied the TTAD technique to study coherence EET in the prototypical conjugated polymer poly[2-methoxy,5-(2′-ethyl-hexoxy)-1,4-phenylene-vinylene] (MEH-PPV). Conjugated polymers have attracted considerable interest because they combine the ease of processing and outstanding mechanical characteristics of polymers with the versatile electrical and optical properties of functional organic molecules (12). EET within and among conjugated polymers is a practical concern as a source of electroluminescence quenching, and is also a fundamental component of how excitation evolves and migrates as a function of chain conformation and packing (13–15). Conjugated polymers are good candidate systems for seeking intermediate coupling effects because the ultrafast evolution of their excited states is governed by the interplay of delocalization and localization (16, 17); moreover, the relative orientation of chromophores is well suited for using anisotropy measurements to detect EET.

In perfectly ordered polymer chains, extensive π-electron conjugation along a rigid backbone confers extraordinary coherence lengths on wave functions (18). Polymers in solution, however, are disordered owing to the relatively low energy barrier for small-angle rotations around bonds along the backbone. Thus, the chain is broken into conformational subunits consisting of planar π-electron systems 2 to 12 repeat units long. These are the primary absorbing units, or chromophores, along an MEH-PPV chain (19) (Fig. 1). Neighboring chromophores are reasonably strongly coupled (20). This electronic coupling dictates how energy is transported among conformational subunits. Two basic types of EET have been identified: intrachain and interchain (20–22). The former consists of energy migration along the backbone between adjacent segments. The latter can be described as energy hopping among segments coupled through space, either because the chains are near to each other in a solid film or because the chain is folded back on itself (Fig. 1).

MEH-PPV polymer chains in two distinct conformations were investigated: (i) solutions in a good solvent (chloroform) where the polymer adopts an extended chain configuration, and (ii) aqueous suspensions of polymer nanoparticles (NPs) formed by individual collapsed chains (23). All experiments were performed in continuously flowing dilute solutions at 293 K (11). The spectra of both samples (fig. S3) exhibited the typical features known for this class of conjugated polymer (24, 25).

The conjugated polymer NPs showed little decay of anisotropy during τ (Fig. 2A), whereas the well-solvated MEH-PPV chains in chloroform showed a striking τ dependence in the TTAD data (Fig. 2B). Owing to the experimental design, this result shows in itself that coherence EET occurs after excitation of extended-conformation MEH-PPV chains, but not in collapsed-chain NPs. Moreover, this phenomenon occurred at room temperature. A qualitative model for the τ dependence of the anisotropy decay can be derived by simulating the anisotropy according to the simplified framework discussed in (11). The anisotropy decay, depending on both τ and T, was modeled for time scales characteristic of coherence and population EET, represented as empirical rate coefficients k_τ and k_T, respectively. Finite pulse duration was taken into account by means of Gaussian field envelopes. Because coherence EET can only be measured when it is followed by population (normal) EET (11), its presence is hidden in the TTAD unless the time scales for the two processes are similar. We find that condition to be easily met when the anisotropy decay is highly nonexponential at early time, as we found for the experimental data (Fig. 2C).

Slices through the experimental surfaces at $\tau = 0$ are plotted in Fig. 3A. It is evident that the anisotropy decays during T more for NPs than for the MEH-PPV in chloroform solution because interchain interactions mediate efficient EET (20). Despite that observation, we saw no coherence anisotropy decay for NPs, which suggests that fluctuations on unconnected conformational subunits are uncorrelated (see below), as is normally assumed. In Fig. 3B, experimental data points as a function of τ are plotted for $T = 0$ and are compared to simulations (solid lines). Owing to
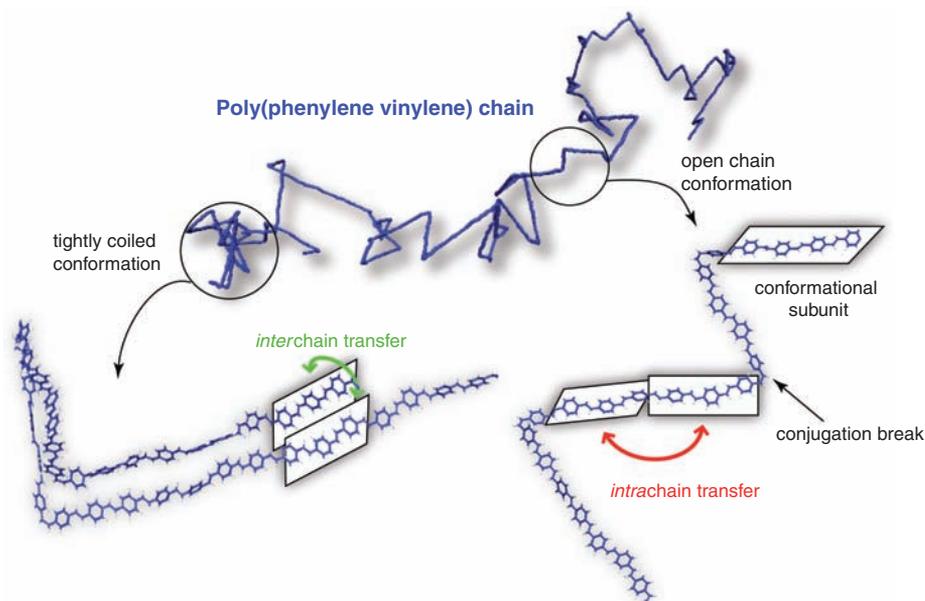

Fig. 1. Example of single-chain conformation of a poly(phenylene vinylene) conjugated polymer, referred as the defect cylinder conformation. Conformational disorder produces a chain of linked chromophores (or conformational subunits) outlined conceptually by boxes. The intrachain EET (migration along the backbone) is the predominant mechanism when the polymer chain assumes an open, extended conformation, typical for solutions in good solvents such as chloroform. On the other hand, interchain interactions (hopping between segments in close proximity) are dominant for tightly coiled configurations, polymer nanoparticles, or films.

the rapid dephasing, in particular because the measurements were performed at 293 K, it was not possible to establish the functional form of the τ dependence (the absolute signal intensities decay strongly with τ, which degrades the signal-to-noise ratio of the anisotropy measurement). Nonetheless, the value that k_τ must assume in order to fit the experimental behavior in the chloroform solution was found to be ~0.05 fs^{-1}, corresponding to a characteristic time of ~20 fs.

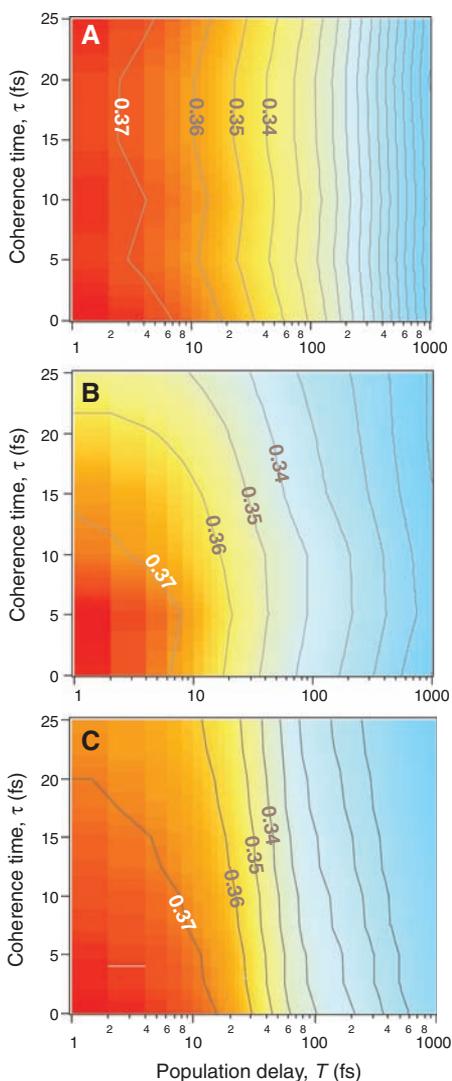We confirmed that the TTAD does not decay for a system that cannot undergo EET by examin-ing a dilute solution of a laser dye, rhodamine 6G in ethanol, absorbing in the same spectral region as MEH-PPV. The experimental data recorded at different τ values confirmed an anisotropy value corresponding to the expected theoretical value of 0.4 for all values of τ and T (Fig. 3B). On substantially longer time scales, the anisotropy of this single chromophore decays with T owing to rotational diffusion in the solution.

Provided that fluctuations of the electronic transition frequencies, ω_{d0} and ω_{a0}, of donor and acceptor chromophores are perfectly correlated, then coherent EET is observed in TTAD as anisotropy decay along τ. That condition is ensured when the correlation function $\xi_{dd}(\tau) \equiv \langle \omega_{d0}(\tau)\omega_{d0}(0) \rangle$ is similar to the cross-correlation function $\xi_{ad}(\tau) \equiv \langle \omega_{a0}(\tau)\omega_{d0}(0) \rangle$. However, if the fluctuations of ω_{d0} and ω_{a0} are uncorrelated (as is usually sup-posed), then $\xi_{ad}(\tau) = 0$ and consequently, according to Kubo's theorems for cumulants (26), coherence EET cannot contribute to the anisotropy decay we measure. Hence, anisotropy as a function of τ in TTAD decays only when coherence EET occurs, in which case $\xi_{ad}(\tau) \neq 0$. The measurement therefore incisively detects evidence for both intermediate-case EET and the necessary correlation of the fluctuations of the donor and acceptor transition frequencies.

The two polymer morphologies described above differ in their dominant energy migration pathways. Interchain EET is expected to be the leading process in the NPs because of the many close chain-chain contacts. In contrast, the rel-atively open and straight conformation adopted by MEH-PPV in chloroform makes intrachain EET dominant. This difference in EET mecha-nism helps to explain why the corresponding TTAD data (Fig. 2) are so strikingly different. For the case of the NPs, the absence of anisotropy decay during τ is likely due to the absence of correlations among the electronic transition frequencies of donor and acceptor chromophores [i.e., $\xi_{ad}(\tau) = 0$]. When these fluctuations are uncorrelated, coherent EET cannot compete with decoherence times of ~10 fs (27). On the other hand, the marked decay of anisotropy with τ for the extended MEH-PPV chains (Fig. 2B) demonstrates that $\xi_{ad}(\tau) \neq 0$—even at ambient temperature—for chromophores con-nected by the conjugated polymer backbone. That result implies that low-frequency vibrations char-acteristic of the polymer backbone have a coher-ence length longer than a single conformational subunit. Clearly it is not sufficient to know only the time scale and amplitude of bath fluctuations (manifest in optical line shapes); it is also important to account for the length scale of those fluctuations.

Our work is consistent with recent observations of protected coherences. Fleming and co-workers have shown, using two-dimensional photon echo (2DPE) experiments, how fluctuations at different chromophore sites in a protein at 77 K can preserve electronic coherences over time scales substantially longer than the decoherence time estimated from the correlation function of the transition frequency (28, 29). Like TTAD, 2DPE is a four-wave mixing experiment in which three laser fields interact with the sample to induce a radiated polarization. The full electric field of the signal is heterodyne-detected by spectral interferometry while T is fixed and τ is scanned. After a Fourier transform with respect to the coherence time τ and the rephasing time t (defined as the evolution time of the signal relative to the arrival time of the third pulse), the two-dimensional electronic spectrum at a given population time T is retrieved (30). The final result is a two-dimensional map in which the sig-nal (real, imaginary, or absolute value) is plotted as a function of the coherence frequency ω_τ, represent-ing the initial excitation, and the rephasing frequency ω_t, which can be interpreted as the ensuing emission.

Experimental and theoretical investigations have stressed that a fundamental characteristic of this technique is its sensitivity to correlations among excited levels (28, 31). We performed 2DPE ex-periments on MEH-PPV solutions in chloroform solvent at 293 K. These studies show that 2DPE yields incisive signatures of electronic coherences between excited states, allowing electronic co-herences to be differentiated from quantum beats that are due to nuclear wave packet motion. Our observation of electronic coherences like $|d\rangle\langle a|$ in MEH-PPV, which are traditionally thought to be
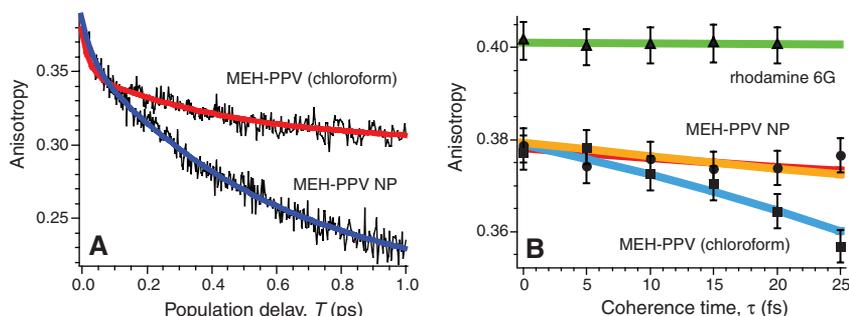

Fig. 2. Two-dimensional plots showing anisotropy decay as a function of τ and T. The color scale indicates the anisotropy, with values shown by the contour lines and corresponding labels. (**A** and **B**) Experimental results for MEH-PPV NP suspension in water (A) and MEH-PPV in chloroform solution (B). (**C**) Simulation results using a multiexponential model to match experimental data for the chloro-form solution with $k_{T1} = 0.05$, $k_{T2} = 0.002$, and a static offset, $k_{\tau1} = 1.0$, $k_{\tau2} = 0.2$, $k_{\tau3} = 0.1$ fs^{-1}. The parameters were not extracted from an optimized fit but were found to provide a reasonable simulation of the data.

Fig. 3. (**A**) Comparison between the conventional ($\tau = 0$) anisotropy decay dynamics in chloroform solution (red) and NP suspension (blue). (**B**) Anisotropy values calculated at $T = 0$ as a function of coherence time for rhodamine 6G (triangles), polymer solution in chloroform (squares), and aqueous NP suspension (circles). The data points are averages; error bars were estimated as SDs of at least nine repeated measurements. The green solid line is a linear fit of the experimental points for rhodamine 6G, whereas the orange, red, and cyan lines represent slices at $T = 0$ of simulations.

Fig. 4. (**A**) Selected 2DPE spectra (real part) of MEH-PPV in chloroform solution at $T = 0$, 40, 110, 140, 160, and 220 fs, demonstrating the oscillation in the amplitude and in the shape of the diagonal peak. The color scale indicates the signal value; deep blue denotes zero, and other values (arbitrary units) are shown by the contour lines and corresponding labels. (**B**) Three-dimensional plot of the amplitude of the spectra along the diagonal line as a function of frequency and population time. A cubic spline interpolation is used to connect the experimental points and generate a smooth surface. (**C**) Comparison between the amplitude of the diagonal peak (left axis, black line) and the ratio between the diagonal and antidiagonal widths of the peak at $1/e$ height (right axis, red line). These data are an average of three independent experiments. The lines show the characteristic anticorrelation theoretically predicted for oscillations caused by electronic coherences.
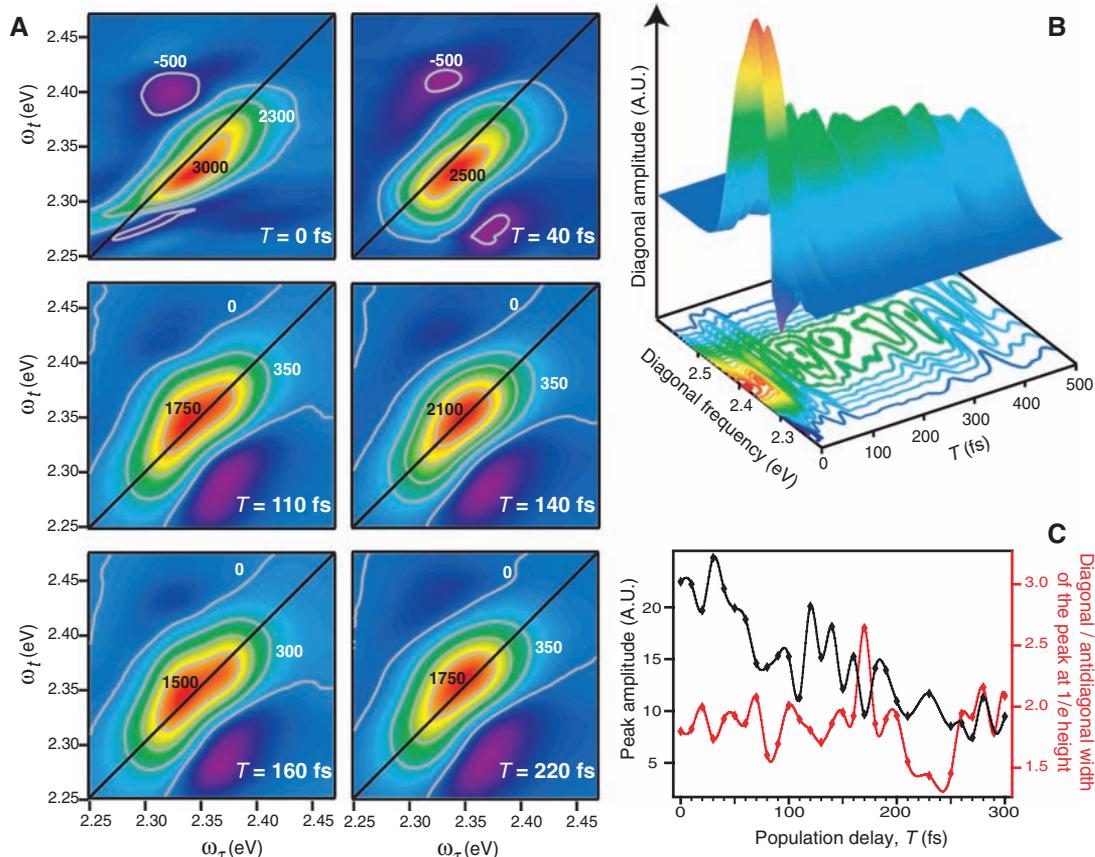
very short-lived owing to decoherence, complement our interpretation of the TTAD data by supporting the condition that $\xi_{ad}(\tau) \neq 0$.

The principal feature in the 2DPE spectra of MEH-PPV solutions in chloroform (Fig. 4A) is a diagonally elongated peak. This diagonal shape, where the radiated signal frequencies (ω_t) are correlated with the initial transition dipole oscillation frequency (ω_τ), is related to the linear absorption spectrum of MEH-PPV. The comparison between 2DPE spectra measured at different T values reveals the presence of an oscillation in the amplitude and in the shape of this main peak, which becomes rounder as it gets stronger. The presence of this oscillation is more evident in the plot of amplitude of the spectra along the diagonal line as a function of frequency and T (Fig. 4B). The electronic origin of these beats is confirmed by the characteristic anticorrelation of the amplitude and the peak shape, defined as the ratio of diagonal to antidiagonal widths of the peak (Fig. 4C). According to previous experimental and theoretical studies, that anticorrelation is a signature of electronic coherences rather than vibrational coherences (28, 31). These electronic beats persist for at least 250 fs, a time period vastly longer than the generally assumed decoherence time of ~10 fs (27).

2DPE is sensitive to coherence effects during T, and therefore it measures the coherent buildup and decay of population while EET is occurring, evidenced by the coherent oscillations in the data.

It establishes that long-lived electronic coherences persist for at least 250 fs after photoexcitation of MEH-PPV in solution at 293 K. The TTAD technique shows unequivocally that coherent EET occurs during τ, which suggests that the electronic coherences observed in the 2DPE data can assist energy migration, predominantly in the case of intrachain EET. It is probable that the common structural framework of the macromolecule introduces correlation in the energy gap fluctuations, which in turn preserves the coherence and permits coherent EET even at room temperature. It remains unclear whether these are predominantly fluctuations affecting the site (diagonal) energies of the conformational subunits, or fluctuations of the electronic couplings (off-diagonal). Physically the former case corresponds to preservation of delocalization by nuclear motions with length scales longer than one conformational subunit. The latter case is more intrinsically related to the formation of conformational subunits, perhaps originating from fluctuations that partially restore a conjugation break.

Our results show that quantum transport effects occur at ambient temperature along conjugated polymer chains. We conclude that chemical bonds connecting chromophores, such as in polymers, macromolecules, and supramolecular systems, play an important role in introducing quantum effects in EET dynamics. This observation extends the paradigm of protein-protected coherences proposed by Fleming and co-workers to chemically bonded chromophores in nanoscale materials at

ambient temperatures. In the case of conjugated polymers, this phenomenon may assist formation of the semiconductor band character of the electronic states.

References and Notes

1. G. D. Scholes, *Annu. Rev. Phys. Chem.* **54**, 57 (2003).
2. S. Rackovsky, R. Silbey, *Mol. Phys.* **25**, 61 (1973).
3. H. Haken, P. Reineker, *Z. Phys.* **249**, 253 (1972).
4. V. M. Kenkre, R. S. Knox, *Phys. Rev. B* **9**, 5279 (1974).
5. V. Chernyak, S. Mukamel, *J. Chem. Phys.* **105**, 4565 (1996).
6. A. Kimura, T. Kakitani, *J. Phys. Chem. B* **107**, 14486 (2003).
7. J. Klafter, R. Silbey, *Phys. Lett.* **76A**, 143 (1980).
8. T. Goodson, *Annu. Rev. Phys. Chem.* **56**, 581 (2005).
9. S. Akimoto, M. Mimuro, *Photochem. Photobiol.* **83**, 163 (2007).
10. C. R. Gochanour, M. D. Fayer, *J. Phys. Chem.* **85**, 1989 (1981).
11. See supporting material on *Science* Online.
12. G. Hadziioannou, G. G. Malliaras, Eds., *Semiconducting Polymers: Chemistry, Physics and Engineering* (Wiley-VCH, Weinheim, Germany, ed. 2, 2007).
13. J. L. Brédas, D. Beljonne, V. Coropceanu, J. Cornil, *Chem. Rev.* **104**, 4971 (2004).
14. A. Ruseckas et al., *Phys. Rev. B* **72**, 115214 (2005).
15. S. Heun et al., *J. Phys. Condens. Matter* **5**, 247 (1993).
16. G. D. Scholes, G. Rumbles, *Nat. Mater.* **5**, 683 (2006).
17. N. S. Sariciftci, Ed., *Primary Excitations in Conjugated Polymers: Molecular Exciton Versus Semiconductor Band Model* (World Scientific, Singapore, 1997).
18. F. Dubin et al., *Nat. Phys.* **2**, 32 (2006).
19. H. Bässler, B. Schweitzer, *Acc. Chem. Res.* **32**, 173 (1999).
20. D. Beljonne et al., *Proc. Natl. Acad. Sci. U.S.A.* **99**, 10982 (2002).

21. T.-Q. Nguyen, J. Wu, S. H. Tolbert, B. J. Schwartz, *Adv. Mater.* **13**, 609 (2001).
22. J. Yu, D. Hu, P. F. Barbara, *Science* **289**, 1327 (2000).
23. C. Szymanski et al., *J. Phys. Chem. C* **109**, 8543 (2005).
24. B. J. Schwartz, *Annu. Rev. Phys. Chem.* **54**, 141 (2003).
25. L. J. Rothberg et al., *Synth. Met.* **80**, 41 (1996).
26. R. Kubo, *J. Phys. Soc. Jpn.* **17**, 1100 (1962).
27. O. V. Prezhdo, P. J. Rossky, *Phys. Rev. Lett.* **81**, 5294 (1998).
28. G. S. Engel et al., *Nature* **446**, 782 (2007).
29. H. Lee, Y.-C. Cheng, G. R. Fleming, *Science* **316**, 1462 (2007).
30. T. Brixner, T. Mancal, I. V. Stiopkin, G. R. Fleming, *J. Chem. Phys.* **121**, 4221 (2004).
31. A. V. Pisliakov, T. Mancal, G. R. Fleming, *J. Chem. Phys.* **124**, 234505 (2006).
32. Supported by an E. W. R. Steacie Memorial Fellowship (G.D.S.) and by the Natural Sciences and Engineering Research Council of Canada. We thank Y.-C. Cheng, G. R. Fleming, and R. J. Silbey for their comments on the manuscript.

A Mouse Speciation Gene Encodes a Meiotic Histone H3 Methyltransferase

Ondrej Mihola,[1]* Zdenek Trachtulec,[1]* Cestmir Vlcek,[1] John C. Schimenti,[2] Jiri Forejt[1]†

Speciation genes restrict gene flow between the incipient species and related taxa. Three decades ago, we mapped a mammalian speciation gene, hybrid sterility 1 (*Hst1*), in the intersubspecific hybrids of house mouse. Here, we identify this gene as *Prdm9*, encoding a histone H3 lysine 4 trimethyltransferase. We rescued infertility in male hybrids with bacterial artificial chromosomes carrying *Prdm9* from a strain with the "fertility" *Hst1[f]* allele. Sterile hybrids display down-regulated microrchidia 2B (*Morc2b*) and fail to compartmentalize γH2AX into the pachynema sex (XY) body. These defects, seen also in *Prdm9*-null mutants, are rescued by the *Prdm9* transgene. Identification of a vertebrate hybrid sterility gene reveals a role for epigenetics in speciation and opens a window to a hybrid sterility gene network.

Hybrid sterility is one of the postzygotic reproduction isolating mechanisms that play an important role in speciation. Hybrid sterility is defined as a situation where parental forms, each fertile inter se, produce infertile offspring (*1*, *2*). Hybrid sterility follows Haldane's rule by affecting predominantly the heterogametic sex (XY or ZW) in crosses where one sex of the progeny is sterile or missing (*3*). Identification of speciation genes has not been particularly successful. Despite decades of effort, only two hybrid sterility genes have been isolated, both from *Drosophila* species (*4*, *5*).

Here, we report identification of a hybrid sterility gene in a vertebrate species. Hybrid sterility 1 (*Hst1*) is one of several genes responsible for spermatogenic failure in *Mus m. musculus–Mus m. domesticus* (*Mmm-Mmd*) hybrids (*6*, *7*). It was genetically mapped to mouse chromosome 17 (Chr17) in hybrids between the *Mmm*-derived PWD/Ph inbred strain (*8*) and several classical laboratory strains, mostly of *Mmd* origin (*9*). Whereas most laboratory inbred strains, including C57BL/6J (B6), carry the *Hst1[s]* (sterility) allele, a few strains, such as C3H/DiSnPh (C3H) or P/J, carry the *Hst1[f]* (fertility) allele (table S1) (*10*). In sterile male hybrids, the *Hst1* interacts, among other genes, with *Hst[ws]* locus on Chr17 of

Mmm subspecies. However, it remains to be determined whether *Hst1* and *Hst[ws]* are identical genes.

A series of high-resolution genetic mapping experiments (*11*–*13*) and haplotype analyses (*14*, *15*) localized *Hst1* to a 255-kb single-copy candidate region on Chr17, harboring six protein-coding genes (*Dll1*, *Pgcc1*, *Psmb1*, *Tbp*, *Pdcd2*, and *Prdm9*) and six pseudogenes (Fig. 1A). To narrow the *Hst1* critical region, we attempted rescue of the hybrid sterility phenotype by transgenesis with bacterial artificial chromosomes (BACs) derived from the C3H/HeJ strain carrying the "fertile" *Hst1[f]* allele. Four overlapping BAC clones (CHORI-34-45F17; hereafter BAC5, CHORI-34-255E14 -BAC19, CHORI-34-289M8 -BAC21, and CHORI-34-331G23-BAC24) (*16*, *17*) were transfected into embryonic stem (ES) cells of (129 × B6)F$_1$, predominantly of *Mmd* origin. The mice with BAC19 did not transmit the BAC to progeny and were not studied further. The other three BACs were transmitted, and as expected, none of them interfered with fertility after outcrossing to the B6
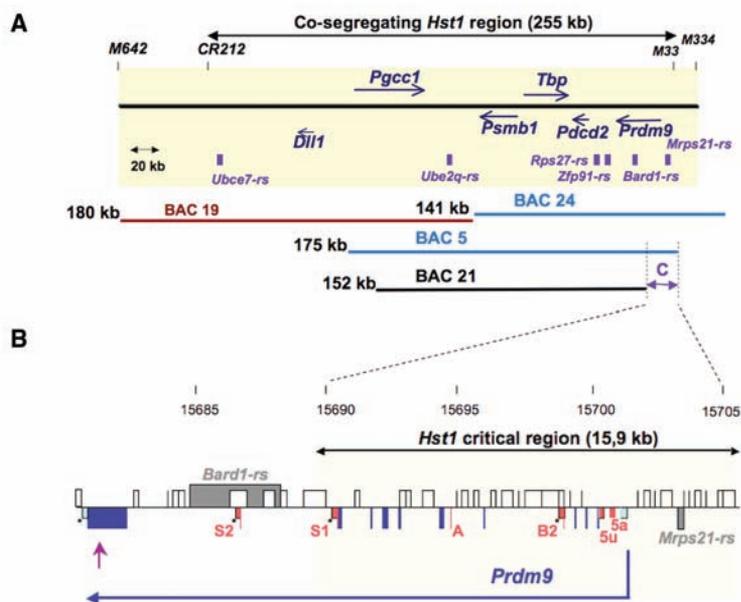

Fig. 1. The *Prdm9* gene encodes *Hst1*. (**A**) The cosegregating *Hst1* region is defined by the markers *CR212* and *M33* (table S2). The arrows point in the direction of gene transcription; the boxes denote pseudogenes. The C3H BAC clones used for transgenesis are shown as horizontal lines with their sizes on the left. The BAC19 chimeras did not transmit the transgene (red line). The blue lines show the BACs rescuing hybrid sterility, whereas BAC21 did not rescue sterility; the C region is necessary for the rescue. (**B**) The *Hst1* critical region. Dark blue boxes: coding exons; light blue box: untranslated region; red boxes: alternative exons (marked 5a, 5u, B2, A, S1, and S2); gray boxes: putative pseudogenes; empty boxes or vertical black lines: repetitive sequences; and asterisks: polyadenylation sites. The vertical arrow points to the site of insertion of a zinc-finger in the last exon of *Prdm9* in the C3H mouse strain. The numbers at the top indicate the positions on Chr17 (in kb, NCBI m37 assembly).

[1]Institute of Molecular Genetics, Academy of Sciences of the Czech Republic, Videnska 1083, 142 20 Prague, Czech Republic. [2]Center for Vertebrate Genomics, Department of Biomedical Sciences, College of Veterinary Medicine, Cornell University, T9014A Vet Research Tower, Ithaca, NY 14853, USA.

*These authors contributed equally to this work.
†To whom correspondence should be addressed. E-mail: jforejt@img.cas.cz